Article

Underwater Acoustic Channel Estimation via an Orthogonal Matching Pursuit Algorithm Based on the Modified Phase-Transform-Weighted Function

Xueru Hu [1,2,3], **Lanyue Zhang** [1,2,3,*], **Di Wu** [1,2,3] and **Jia Wang** [1,2,3]

1   National Key Laboratory of Underwater Acoustic Technology, Harbin Engineering University, Harbin 150001, China
2   Key Laboratory of Marine Information Acquisition and Security (Harbin Engineering University), Ministry of Industry and Information Technology, Harbin 150001, China
3   College of Underwater Acoustic Engineering, Harbin Engineering University, Harbin 150001, China
*   Correspondence: zhanglanyue@hrbeu.edu.cn

Abstract: In the context of torpedo guidance systems, the performance of active sonar in channel parameter estimation and target detection and recognition is significantly degraded by the multipath effect and the time-varying characteristics of the underwater acoustic (UWA) channel. Therefore, it is urgent to propose an algorithm that can accurately estimate the channel parameters in multipath time-varying UWA channels. To solve these problems, this study developed a modified phase transform (PHAT)-weighted function and applied it to the orthogonal matching pursuit (OMP) algorithm, named M-PHAT-OMP. The proposed algorithm is more robust, improves the resolution of the time delay and further improves the estimation accuracy of the parameters in the case of motion. Furthermore, with the aim of solving the problem of the difficulty that the traditional OMP algorithm has in determining sparsity, this study proposes a joint-threshold method, where the threshold value serves as the condition for terminating the algorithm's iteration. The simulation results demonstrate that the M-PHAT-OMP algorithm proposed in this study exhibits a superior performance compared to other algorithms, as evidenced by its lower root mean square error (RMSE) for delay. Moreover, the experimental results also validate that the proposed algorithm has superior robustness and resolution of the time delay in practical applications.

Keywords: sparse-channel estimation; frequency estimation; weighted function; modified PHAT-weighted orthogonal matching pursuit algorithm (M-PHAT-OMP)

1. Introduction

The underwater acoustic channel exhibits extremely complex characteristics, which will generate coherent multipath signals when sound waves undergo the effects of interfaces and scatter. Due to the slow speed of sound waves, any movement of the platform will cause a Doppler effect that cannot be ignored [1,2]. Therefore, the underwater acoustic channel is a type of dual-propagation (time and frequency) channel. Moreover, the scattering of the irregular seabed terrain and the influence of the wind and waves at the sea's surface cause the channel to exhibit time-varying characteristics [3]. Currently, underwater sensing applications, such as ocean detection, seabed surveillance and acoustic early warning systems [4], which use acoustic waves as a transmission medium, are subject to the aforementioned characteristics of the channel. These can result in signal distortion, energy attenuation and other issues that ultimately affect the accuracy of the system's output. Therefore, it is crucial to accurately estimate the parameters of the underwater acoustic channel. The purpose of channel estimation is to use the appropriate means to enhance the compatibility between the detection system and the marine environment, as well as

improve the efficiency and reliability of target detection based on the estimated characteristics of the underwater acoustic channel. This study presents an OMP algorithm based on the modified PHAT-weighted function, which improves the accuracy of the estimation and robustness of the algorithm.

Real channels have sparse characteristics; that is, most of the channel's energy is concentrated around a few delay and/or Doppler values [5], thereby reducing the unknowns of the channel estimation. Conventional channel estimation algorithms, such as least squares (LS) [6,7], minimum mean square error (MMSE) [8] and linear minimum mean square error (LMMSE) [9], ignore the sparsity of real underwater acoustic channels [10]. When the signal-to-noise ratio (SNR) is low, the estimated error of these algorithms increases significantly, and they cannot meet the performance requirements of the increasingly more sophisticated underwater acoustic systems. With the development of the sparse characteristics of the UWA channel, sparse recovery algorithms based on compressed sensing have become an important research direction in the field of channel estimation [11–15], the most representative of which is the orthogonal matching pursuit (OMP) algorithm [10,16]. Nevertheless, this method still has some limitations. The sparsity determines the number of iterations and the estimation accuracy of the algorithm. The size of the dictionary matrix [17–19] determines the computation amount and estimation accuracy of the algorithm. For example, if the dictionary matrix is not complete, then the inaccurate selection of the dictionary's column atoms during the updating process may result in the failure of the reconstruction. If the dictionary is too comprehensive, then the inner product between the observation vector and the dictionary's column atoms will increase the computation [20], thereby reducing the real-time performance of the algorithm in the iterative process. Additionally, in the presence of a low SNR, the algorithm's performance deteriorates, as the selection of the sparsity value relies upon experience, and it is crucial to establish appropriate termination conditions for running the algorithm. At present, many scholars have proposed improved algorithms with better performances based on conventional OMP algorithms. To enhance the algorithm's efficiency and optimize the runtime, Hu et al. introduced a low-complexity OMP search method that used coarse-to-fine grid searches [20]. However, this method assumed equal amplitudes of the elements in the channel's coefficient vector, which was impractical. To address this issue, Yu et al. utilized FFT to compute the inner products, and proposed an OMP algorithm based on fast block Fourier transform [21], which reduced the computational complexity while maintaining the same performance as the original OMP algorithm. Wan et al. [22] derived a closed-form path-delay estimate for OMP channel estimation, which utilized the characteristic of the Hermitian inner product between the pilot-compensated frequency vector of the observation and the columns of the dictionary matrix, and proposed a two-step scheme to search the samples in the closed-form estimation to further reduce the computational complexity. Ma et al. [23] proposed an OMP algorithm based on interpolation that utilized the calculated frequency domain, resulting in improved accuracy in its estimations of the path delay while maintaining low computational complexity. To avoid repeated calculations in each iteration of the traditional OMP method, Gang et al. precomputed the Hermitian inner-product matrix for the candidate path signatures [24]; the path gain only needed to be estimated once using the LS algorithm at the end of the iteration, which reduced the demands of computation. Chunguo Li et al. [25] correctly calculated the cost function of OMP by using the pilot length and the number of pilot blocks, thereby greatly reducing the complexity of sparse-channel estimation in the OMP. An algorithm that employed physical sparsity to determine the termination condition [26] suffered from a limited estimation accuracy under high-level noise and had difficulty balancing the accuracy of the estimation and the computational cost at low noise levels. To address this issue, an adaptive OMP algorithm was proposed [27]. On the basis of the sparsity adaptive matching pursuit (SAMP) algorithm, Zhang et al. [28] proposed an adaptive-step SAMP algorithm, which realized the algorithm without prior knowledge of the channel's sparsity. The step size was adjusted adaptively to approximate the true dilution, thereby improving the accuracy of the channel estimation. Quan et al. [29]

applied the Gram–Schmidt method to resolve the delay–Doppler parameters during the matching iterations of tracking, which avoided the computational complexity of inverting a matrix and enhanced the robustness and effectiveness of estimating the delay–Doppler parameters. Zuofu Wang et al. [30] proposed a synchronous orthogonal matching pursuit algorithm based on exponential smoothing (ES-SOMP). The algorithm first uses the recovery algorithm based on a joint-sparse model to estimate the UWA channel, and then it models the problem of channel estimation as a joint-sparse recovery problem. It then uses the exponential smoothing method to de-noise the estimated channel. The results of the simulation showed that the performance of the algorithm was improved by 2–3 dB compared with the traditional OMP and SOMP algorithms.

As can be seen from the above, most OMP algorithms have been studied according to how to reduce the computational complexity and choose the appropriate sparsity. Considering the above two factors, this study proposes an OMP algorithm based on the modified PHAT-weighted function to further improve the accuracy of the estimation and the robustness of the algorithm. In this algorithm, the traditional OMP algorithm's inner-product process for selecting the best atomic index is replaced by the FFT method, which reduces the computational burden [21]. In addition, on the basis of the frequency-domain calculations above, we also utilized the generalized cross-correlation (GCC) algorithm [31] of the improved PHAT-weighted function to enhance the resolution of the time delay. At the same time, an adaptive threshold was used to filter the channel parameter information, reducing the estimation errors. Through numerical simulation and an analysis of the experimental data, it was verified that the proposed algorithm exhibited superior estimation accuracy for both static and dynamic targets.

The rest of this study is organized as follows. In Section 2, we present the system model and the theoretical foundation, and show the theoretical derivation of the OMP algorithm based on the modified PHAT-weighted function. Section 3 analyzes the performances of different weighted functions for estimating the time delay and explores the characteristics of the M-PHAT-OMP algorithm in the case of stationary and moving sources of sound. In Section 4, we describe an experiment carried out in Lake Qiandao, and the test results are analyzed to show the feasibility of the proposed algorithm. Finally, the conclusions are given in Section 5.

2. Materials and Methods

2.1. System Model

In this study, the UWA channel was assumed to be a linear time-invariant coherent multipath sparse channel in one observation period. The channel can be described by a time-invariant filter with a sparse tap distribution. In the coherent multipath channel model, the sound wave is transmitted from the transmitting transducer and reaches the hydrophone through multiple paths that are reflected by the boundaries. The signal received by the hydrophone is the superposition of the signals from different paths, so it will have different degrees of distortion and fading compared with the original signal. If we assume that the total number of acoustic paths is L, then the amplitude of the path l is α_l, the time delay is τ_l and the impulse response function of the underwater acoustic multipath channel is as follows:

$$h(t) = \sum_{l=1}^{L} \alpha_l \delta(t - \tau_l) \tag{1}$$

The transmitted signal ($s(t)$) propagates through the underwater acoustic channel to the receiver, and the received signal ($y(t)$) can be expressed as follows [32]:

$$y(t) = s(t) * h(t) + w(t) = \sum_{l=1}^{L} \alpha_l s(t - \tau_l) + w(t), \ (i = 1, 2, \cdots, N) \tag{2}$$

where $*$ represents the convolution operation, and $w(t)$ is the Gaussian white noise with a mean value of zero. However, discrete sampling points are commonly utilized to replace continuous analog signals in practice. The discrete form of the received signals is as follows:

$$y[m] = \sum_{k=0}^{N-1} s[m-k]h[k] + w[m], \; m = 0, \ldots, M-1 \qquad (3)$$

$$y[m] = y(m\Delta t), \; m = 0, \ldots, M-1 \qquad (4)$$

$$s[m] = s(m\Delta t), \; m = 0, \ldots, M-1 \qquad (5)$$

where $h[m], (m = 1, \ldots, N-1)$ represents the impulse response of the channel; N represents the length of the channel; M represents the length of the observation window; $y[m]$ and $s[m]$ are the discrete received and transmitted signals, respectively; and $w[m]$ is the discrete additive noise. Equation (3) can be expressed in matrix form as follows:

$$
\begin{bmatrix} y[0] \\ y[1] \\ \vdots \\ y[M-1] \end{bmatrix} =
\begin{bmatrix} s[0] & s[-1] & \cdots & s[-N+1] \\ s[1] & s[0] & \cdots & s[-N+2] \\ \vdots & \vdots & \vdots & \vdots \\ s[M-1] & s[M-2] & \cdots & s[M-N] \end{bmatrix}
\begin{bmatrix} h[0] \\ h[1] \\ \vdots \\ h[N-1] \end{bmatrix} +
\begin{bmatrix} w[0] \\ w[1] \\ \vdots \\ w[M-1] \end{bmatrix} \qquad (6)
$$

Equation (6) can be simplified as follows:

$$\boldsymbol{y} = \boldsymbol{Ah} + \boldsymbol{w} \qquad (7)$$

where A is defined as a Toeplize matrix with $M \times N$ dimensions composed of the sending signals; it is also called the dictionary matrix or observation matrix:

$$
\boldsymbol{A} =
\begin{bmatrix} s[0] & s[-1] & \cdots & s[-N+1] \\ s[1] & s[0] & \cdots & s[-N+2] \\ \vdots & \vdots & \vdots & \vdots \\ s[M-1] & s[M-2] & \cdots & s[M-N] \end{bmatrix} \qquad (8)
$$

Due to the sparsity of the underwater acoustic channel, most components of the impulse response in the multichannel are zero. Therefore, the task of estimating the underwater acoustic channel can be solved by a compressed sensing algorithm.

2.2. Generalized Cross-Correlation Algorithm

The conventional OMP algorithm has strict requirements regarding the dictionary matrix. Incomplete elements of the dictionary matrix can cause serious errors or even cause the estimation to fail, while a too-complete dictionary matrix can increase the computational demand. To solve this problem, this study proposed a GCC algorithm with a weighted function, based on the frequency-domain calculation method [23], to obtain the information on the time delay corresponding to the maximum value in each iteration. According to this information, the optimal atomic sequence in this iteration can be constructed. If we assume that $x(t)$ is the transmitting signal and $y(t)$ is the receiving signal, then the expression for the GCC function ($R_{xy}(\tau)$), given the signals $x(t)$ and $y(t)$, is as follows:

$$R_{xy}(\tau) = \int_{-\infty}^{+\infty} \phi_{xy}(\omega) X(\omega) Y^*(\omega) e^{-j\omega\tau} d\omega \qquad (9)$$

where $(\cdot)*$ represents the complex conjugate. The calculation process is shown in Figure 1.
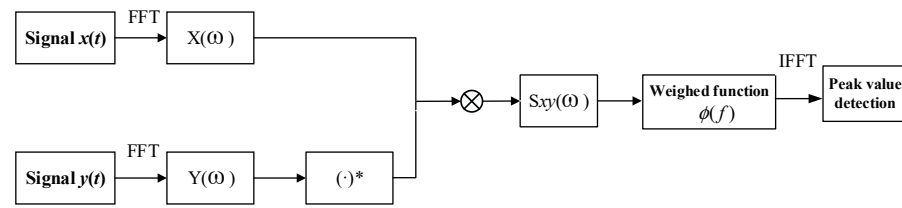
Figure 1. Calculation process for estimating delay using GCC.

The cross-correlation function can be obtained by performing an inverse Fourier transform on the cross-power spectral density function of two signals. The utilization of fast Fourier transform accelerates the speed of the computation, thereby enhancing the real-time performance of the GCC algorithm. The resolution of the delay in the basic GCC algorithm is reduced when the signal contains a strong spectral component. The weighted function serves as a pre-filter for the signal, effectively enhancing the spectral components of the response while suppressing those of the noise, thereby improving the resolution of the delay. The conventional weighted functions commonly used are shown in Table 1 [33].

Table 1. Conventional weighted functions.

Function	ROTH	SCOT	PHAT	HB
$\phi(\omega)$	$\frac{1}{S_{xx}(\omega)}$ or $\frac{1}{S_{yy}(\omega)}$	$\frac{1}{\sqrt{S_{xx}(\omega)S_{yy}(\omega)}}$	$\frac{1}{\left|S_{xy}(\omega)\right|}$	$\frac{\left|S_{xy}(\omega)\right|}{S_{xx}(\omega)S_{yy}(\omega)}$

In Table 1, $S_{xx}(\omega)$ and $S_{yy}(\omega)$ are the self-power spectra of the signals $x(n)$ and $y(n)$, respectively, while $S_{xy}(\omega)$ is the cross-power spectrum of signal $x(n)$ and signal $y(n)$. The ROTH function effectively suppresses the regions of frequency with high noise levels, but it exhibits the phenomenon of expansion, and its applicability is limited. Based on the ROTH function, the SCOT function considers the impact of both signals on the cross-correlation results. However, when the densities of the power spectra of the received signals in two channels are identical, false peaks may occur. The HB function pre-whitens the input signal by normalizing its self-power spectrum, thereby reducing errors. However, when the SNR is low, the performance of the HB algorithm decreases. The PHAT function acts as a whitening filter, sharpening the peak of the cross-correlation function. However, when the signal's power is the lowest, the numerator approaches zero, resulting in an increase in the error of calculation.

2.3. Modified PHAT-Weighted Function

In order to solve the problem of the sharp decrease in the performances of the weighted functions above at a low SNR, this study proposed an improved PHAT-weighted function [34], which is denoted M-PHAT. The expression of the weighted function is as follows:

$$\phi_{M-PHAT}(\omega) = \frac{\left|\gamma_{xy}(\omega)\right|}{\left|S_{xy}(\omega)\right|^{\alpha} + \beta} \tag{10}$$

where $\left|\gamma_{xy}(w)\right|$ is the modular coherent function, which is expressed as follows [33]:

$$\left|\gamma_{xy}(\omega)\right| = \frac{\left|S_{xy}(\omega)\right|}{\sqrt{S_{xx}(\omega) \cdot S_{yy}(\omega)}} \tag{11}$$

By substituting the modulus coherence function into the M-PHAT-weighted formula, we obtain the following equation:

$$\phi_{M-PHAT}(\omega) = \frac{|S_{xy}(\omega)|}{\sqrt{S_{xx}(\omega) \cdot S_{yy}(\omega) \cdot (|S_{xy}(\omega)|^\alpha + \beta)}} \tag{12}$$

The modulus coherence function includes the cross-correlation of the two signals, and when the signal's energy is low, the weight is reduced correspondingly to suppress the noise. In Equation (12), the exponent α is used to reduce the negative impact caused by a signal with too little power, improve its capacity for suppressing spurious peaks in low-SNR scenarios and reduce the impact of noise on the estimation of the delay. The value of α ranges from 0 to 1. When $\alpha = 0$, it is equivalent to the product of the basic window function with a constant weight and the modular coherence function, but the resolution is poor. When $\alpha = 1$, the weighted function is the product of the PHAT-weighted function and the modulus coherence function, which is greatly affected by noise. In order to find a weighted function with good anti-noise performance and strong stability, a certain amount of resolution is sacrificed, and a value between 0 and 1 is selected. When the signal energy is weak, a constant ($\beta(\beta > 0)$) is introduced into the denominator of the weighted function to prevent large errors caused by the denominator approaching zero.

According to the K-fold verification method, when $\alpha = 0.75$ and $\beta = 1$, the anti-noise performance of the algorithm has achieved the ideal effect; thus, these two values were selected as constants in the function.

The performance of the algorithm for estimating the time delay is usually quantified according to its accuracy (R_{ac}) and root mean square error *(RMSE)* (R_{RMSE}). The expressions of the R_{ac} and R_{RMSE} are as follows:

$$R_{ac} = \frac{N_{correct}}{N} \times 100\% \tag{13}$$

$$R_{RMSE} = \sqrt{\frac{1}{N \times L}\sum_{i=1}^{N}\sum_{j=1}^{L}(\tau_{ij} - \tau_{0j})^2} \tag{14}$$

In Equation (13), $N_{correct}$ is the number of correct estimates; when the estimated value is consistent with the real value, it is recorded as a correct estimate. N is the total number of estimates, L is the number of acoustic paths, τ_{0j} is the jth element in the real-delay vector and τ_{ij} is the jth element of the delay vector in the ith estimation. When there is only one channel delay, Equation (14) can be simplified to the following:

$$R_{RMSE} = \sqrt{\frac{1}{N}\sum_{i=1}^{N}(\tau_i - \tau_0)^2} \tag{15}$$

2.4. The OMP Algorithm Based on Modified PHAT Weighting (M-PHAT-OMP)

In this part, we introduce the M-PHAT-weighted function into the traditional OMP algorithm, which is called M-PHAT-OMP. The calculation steps of the classical OMP algorithm are introduced in reference [24]; thus, they will not be detailed in this paper. One of the steps of the classical OMP algorithm is to calculate the inner product between the observed signal and each column vector in the dictionary matrix, which is equivalent to performing a time-domain cross-correlation calculation, and the column index corresponding to the maximum value is extracted for updating the index set. Previously, this study analyzed the advantages of weighted GCC over the time-domain cross-correlation algorithms. Therefore, we used the M-PHAT-weighted GCC algorithm to replace the time-domain cross-correlation, which reduced the computational burden, enhanced the accuracy of the estimation and improved the resolution of the time delay.

The M-PHAT-weighted algorithm has the property of clustering near the real time delay, and the maximum value in each cluster is the current estimated value. The M-PHAT-OMP algorithm utilizes the clustering characteristics of the M-PHAT-weighted algorithm to compute its energy value through a sliding-window approach. The range of the delay is determined by finding the maximum value of the energy, and the delay corresponding to the maximum value in this range is used as the optimal value for each iteration, which effectively eliminates any outliers and makes the algorithm more robust. The LS algorithm is used to estimate the amplitudes of the selected delay in each iteration. The jointly estimated amplitude, shown in Step 7, is used as the threshold, and the information on the delay corresponding to the threshold value is retained until the iteration terminates.

The specific steps of the M-PHAT-OMP algorithm are shown in Algorithms 1.

Algorithms 1. The specific steps of the M-PHAT-OMP algorithm.

Input:
　　Received signal $\boldsymbol{y}$; dictionary $\boldsymbol{D} = [d_1 \quad d_2 \quad \cdots \quad d_N]$;
　　maximum number of iterations K; pre-measured noise amplitude modulus $|A_{noise}|$.
Initialization:
　　Residual signal: $\boldsymbol{r}_0 = \boldsymbol{y}$; index set: $\boldsymbol{\Lambda} = \varnothing$; rebuild atomic: $\boldsymbol{\Phi}_0 = \varnothing$;
　　iteration number: $k = 0$
Iterative process:
　　Step 1: $k = k + 1$
　　Step 2: Find the most matched atomic sequence index (λ_k).
　　　　Using the M-PHAT-weighted GCC method to calculate the cross-correlation,
　　　　value ($R_{\langle D_i, r_{k-1} \rangle}(\tau)$) of the residual ($\boldsymbol{r}_k$) and dictionary sequence ($\boldsymbol{D}_i$), add a
　　　　sliding window to the $R_{\langle D_i, r_{k-1} \rangle}(\tau)$ and calculate the energy value in the window.
　　　　When the energy reaches its maximum, this corresponds to a range of delay,
　　　　and the maximum modulus within this range is selected as the maximum value
　　　　of the current cross-correlation sequence, denoted $R_{D_i, r_{k-1}}$. The column index (λ_k)
　　　　corresponding to the best atom is as follows:
$$\lambda_k = \mathrm{argmax}(|R_{D_i, r_{k-1}}|), \ i = 1, 2, \cdots, N$$
　　　　where $\boldsymbol{D}_i$ represents the ith column of the observation matrix $\boldsymbol{D}$.
　　Step 3: Update the index sets and rebuild the atomic sets:
$$\begin{cases} \boldsymbol{\Lambda}_k = \boldsymbol{\Lambda}_{k-1} \cup \lambda_k \\ \boldsymbol{\Phi}_k = \boldsymbol{\Phi}_{k-1} \cup \boldsymbol{D}_{\lambda k} \end{cases}$$
　　Step 4: Use the LS algorithm to estimate the channel's impulse response (CIR):
$$\hat{h}_k = \left(\boldsymbol{\Phi}_k^H \boldsymbol{\Phi}_k\right)^{-1} \boldsymbol{\Phi}_k^H \boldsymbol{y}$$
　　Step 5: Update the signal's residuals according to the CIR estimates:
$$\boldsymbol{r}_k = \boldsymbol{y} - \boldsymbol{\Phi}_k \hat{h}_k$$
　　Step 6: Judgment: if $k = K$, then stop the iteration and perform Step 7; otherwise, repeat
Steps 1–5.
　　Step 7: Select the component in $\hat{h}$ that satisfies $\left|\hat{h}\right| < \max(|A_{noise}|, \alpha \times mean(|\hat{h}|))$ as the final
estimated value.
Output: The estimated value of the CIR, $\hat{h}$.

---

3. Results and Analysis of the Simulation

This section presents some simulations to validate the proposed algorithms. Section 3.1 analyzes the performance of the modified PHAT (M-PHAT)-weighted algorithm, including the performances of the GCC algorithms based on different weighted functions under the conditions of a single-path channel and multipath channel with small differences in the delay. Section 3.2 evaluates the performance of the M-PHAT-OMP algorithm under the scenarios of static and dynamic sound sources.

The frequency of the torpedo homing signal is mostly higher than 20 kHz. Moreover, the common forms of the torpedo homing signal include the single-frequency pulse signal, frequency-modulated pulse signal and so on; thus, this study chose the high-frequency CW pulse signal for research.

3.1. Analysis of the Performance of the Modified PHAT-Weighted Algorithm

The performances of the GCC algorithms based on different weighted functions were analyzed under the conditions of a single-path channel and multipath channel with small differences in the delay.

3.1.1. Estimation of Time Delay with Single-Path Model

To evaluate the algorithm's performance with a single-path channel, this study established a channel model with only one delay and generated the received signal based on this model. The statistics of the performances of the algorithms were evaluated through a Monte Carlo simulation conducted at various levels of the signal-to-noise ratio (SNR). We defined the SNR as $10\lg(\sigma_s/\sigma_n)$, where σ_s and σ_n represent the power of the signal and noise, respectively. Then, we determined the R_{ac} and R_{RMSE} of each algorithm at different SNRs. The parameters of the transmitted signal and channel in the simulation are shown in Table 2. The curves of the variation in the simulation results with the levels of the SNR are shown in Figure 2.

Table 2. Parameters of the single-path channel simulation.

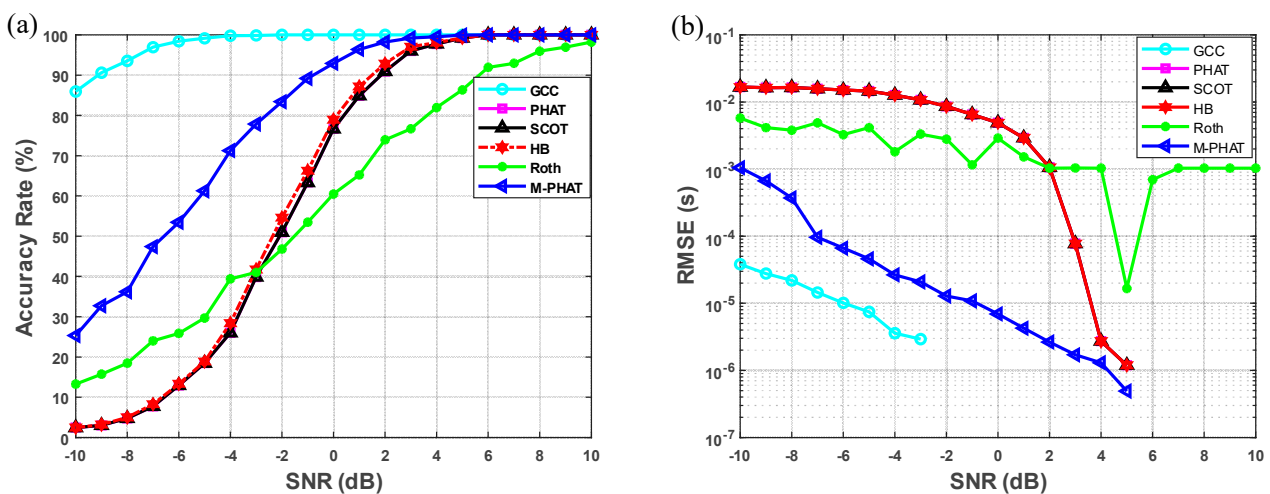| Transmitted Signal Parameters				Received Signal Parameters	Information on Time Delay
Signal Type	Pulse Width	Frequency	Pulse Period	Sampling Rate	Time Delay
CW pulse	40 ms	25 kHz	500 ms	262.144 kHz	32 ms

Figure 2. (**a**) Accuracy of the estimated time delay under different SNRs. (**b**) RMSE of the estimated time delay under different SNRs.

When estimating the delay in a single-path channel, the estimated value of the delay is determined by identifying the index of the maximum cross-correlation function. The traditional GCC algorithm exhibited the best performance, as the resolution of the delay was not taken into consideration, but the M-PHAT function proposed in this study had a better performance in terms of estimation than the other weighted functions. Figure 2a shows that the performances of the PHAT, SCOT and HB functions were almost the same. When the SNR was lower than 0 dB, the R_{ac} of these functions dropped sharply with a decrease in the SNR. Although the downward trend of the ROTH function exhibited relative stability with a decrease in the SNR, its correct rate was lower than that of the M-PHAT function at the same SNR. Compared with the ROTH function, the performance of the M-PHAT function improved by approximately 4 dB. In this study, when the estimated value aligned perfectly with the true value, the estimation was deemed to be accurate. The

evaluation criteria were relatively stringent; thus, the RMSE may more accurately reflect the algorithm's performance in practical applications. In Figure 2b, the PHAT, SCOT and HB functions performed the same, and their R_{RMSE} values were always higher than that of the M-PHAT algorithm; the R_{RMSE} of the ROTH function at a low SNR was smaller than that of the PHAT and the other two functions but was still higher than that of the M-PHAT function. The results of the simulation showed that the M-PHAT function had the best performance, except for the GCC, with the single-path channel model.

3.1.2. Estimation of Time Delay in Multipath Model

In a multipath underwater acoustic channel from a shallow sea, there is a small difference in the delay between the direct sound and the reflected sound from the sea's surface when the receiving hydrophone is positioned near the surface. It was expected that the algorithm would still effectively separate the two lines of sound in the presence of a low SNR. The algorithm requires a higher resolution of the delay at a low SNR.

To verify the capability of the algorithm to resolve the time delay in this case, a simulation for estimating the time delay was performed for multipath channels with delays of 32 ms and 32.2 ms. The parameters of the transmitted and received signals are shown in Table 2. The received signal was added to Gaussian white noise with an SNR of −5 dB, and the results of the algorithm's estimation are illustrated in Figure 3.
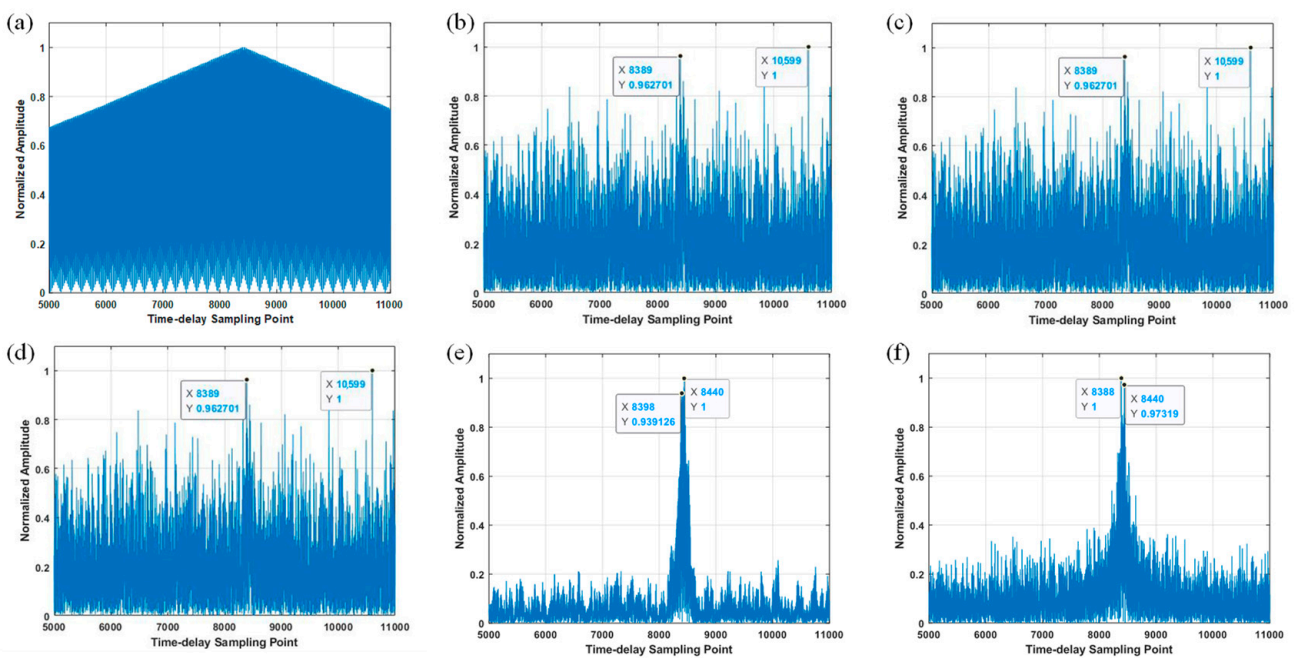

Figure 3. GCC algorithms based on different weighted functions when the SNR was −5 dB: (**a**) GCC algorithm; (**b**) PHAT-weighted algorithm; (**c**) SCOT-weighted algorithm; (**d**) HB-weighted algorithm; (**e**) ROTH-weighted algorithm; (**f**) M-PHAT-weighted algorithm.

As illustrated in Figure 3, when the relative delay of the multipath was small, the basic GCC algorithm only presented a single peak, which failed to differentiate the multipath at an SNR of −5 dB. The estimation results of the commonly used PHAT-, SCOT- and HB-weighted algorithms were affected by noise and had multiple false peaks, making it difficult to accurately determine the correct delay. The ROTH-weighted algorithm estimated two path delays; however, there were estimation errors. The M-PHAT algorithm proposed in this study still accurately identified two closely spaced delays by extracting the local extrema. The results of the simulation provided full verification that the M-PHAT function maintained a better resolution of the time delay, even under low-SNR conditions.

According to the parameters of the simulation above, this study used the Monte Carlo simulation method to calculate the statistics of the R_{ac} and R_{RMSE} for each algorithm at different SNRs. The results of the simulation are as shown in Figure 4.
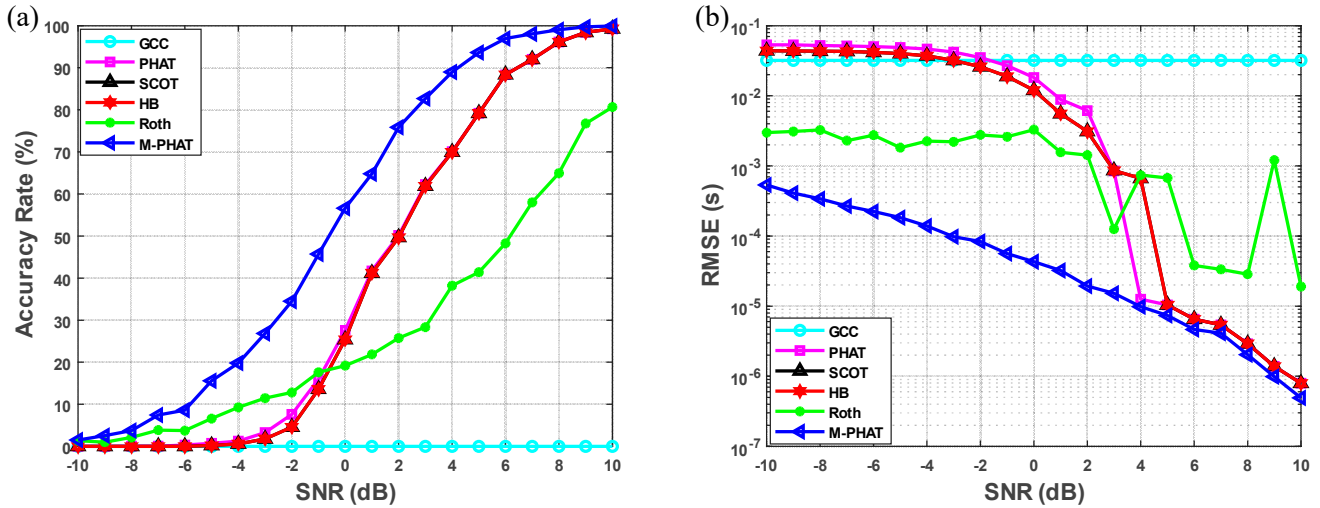

Figure 4. (**a**) Correct rates of the estimated delay under different SNRs. (**b**) *RMSEs* of the estimated delay under different SNRs.

Figure 4a shows the estimated accuracy of each algorithm with the various SNRs, from which it can be seen that the M-PHAT function proposed in this study had the highest accuracy. Its accuracy rate exhibited a tendency of rapid initial progress, followed by slower progress as the SNR increased. Because the GCC function can only estimate a single delay, the accuracy of its estimation (R_{ac}) was zero, regardless of the SNR. The R_{ac} values of the PHAT, SCOT and HB functions were almost the same, and their curves were lower than that of the M-PHAT function. When the SNR was greater than −2 dB, the R_{ac} of the M-PHAT function was approximately 3 dB higher than those of the aforementioned three functions. The accuracy of the ROTH function was approximately linearly related to the SNR, but it was still lower than that of the M-PHAT function. When the SNR was lower than 6 dB, the difference between the accuracies of the two functions increased with an increase in the SNR, and the maximum difference was 50%. Figure 4b shows the *RMSEs* of the estimated delay of various weighted functions under different SNRs. The M-PHAT function exhibited the lowest *RMSE* across all SNR levels and performed optimally. When the SNR fell below 4 dB, the *RMSE* of the M-PHAT function reduced by two orders of magnitude compared with those of the PHAT, SCOT and HB functions. Furthermore, the overall *RMSE* reduced by an order of magnitude compared with the ROTH function. In conclusion, the simulation verified that the M-PHAT function exhibited a superior resolution of the delay and robustness under low SNR levels.

3.2. Analysis of the Performance of the M-PHAT-OMP Algorithm

The performance of the M-PHAT-OMP algorithm was analyzed through simulations in which the receiver hydrophone remained stationary, and the sound source was either fixed or moving.

3.2.1. Evaluation Indicators

In order to evaluate the performance of the algorithm, this study adopted an assessment criterion: the regional focalization degree (RFD), which is defined as follows:

$$\text{RFD}_{r_1, r_2} = \frac{\sum_{(i,j) \in \Omega_{r_1, r_2}} \overline{\mathbf{Y}}_{ij}^2}{\sum_i \sum_j \mathbf{Y}_{ij}^2} \tag{16}$$

where $\Omega_{r_1,r_2} = \left\{ (i,j) \middle| \mathbf{Y}_{i'j'} \neq 0, |i'-i| \leq r_1, |j'-j| \leq r_2 \right\}$ represents the set of coordinates covered by all non-zero regions in **Y**, and r_1 and r_2 are non-negative integers representing the size of the local region around the coordinates of the non-zero values in the matrix (**Y**). We set $r_1 = r_2 = 10$ in this study. The higher the value of the RFD, the more accurate the algorithm.

When there is a relative motion between the sound source and the receiving hydrophone, it is necessary to consider the delay-scaled spread function (DSSF) [35,36], which contains the time delay, Doppler scale and amplitude. We adopted the normalized mean squared error of the DSSF (NMSE$_{\text{DSSF}}$) as the performance metric to measure the estimation.

$$\text{NMSE}_{\text{DSSF}} = \frac{\sum\limits_{m}\sum\limits_{n}\left|\hat{\mathbf{H}}[m,n] - \mathbf{H}[m,n]\right|^2}{\sum\limits_{m}\sum\limits_{n}\left|\mathbf{H}[m,n]\right|^2} \tag{17}$$

Here, $\mathbf{H}[m,n]$ is the DSSF, and $\hat{\mathbf{H}}[m,n]$ is the estimation of the $\mathbf{H}[m,n]$.

The channel's power-delay profile (PDP) [37] contains crucial information about the channel, including the path intensity, density and distance between the transmitter and the receiver, or between the detector and the target. Therefore, the PDP is a very important assessment criterion. The PDP can be obtained by reducing the dimensions of the DSSF, which means removing the scale dimension. The normalized mean squared error of the power-delay profile (NMSE$_{\text{PDP}}$) can be expressed as follows:

$$\text{NMSE}_{\text{PDP}} = \frac{\sum\limits_{n}\left|\sum\limits_{m}\hat{\mathbf{H}}[m,n] - \sum\limits_{m}\mathbf{H}[m,n]\right|^2}{\sum\limits_{n}\left|\sum\limits_{m}\mathbf{H}[m,n]\right|^2} \tag{18}$$

3.2.2. Fixed Source

Simulation 1: Analyzing the resolution of the delay of the proposed algorithm under conditions with small differences in the delay

Assuming that the position of the receiving/transmitting equipment was fixed, we used Bellhop software based on the ray model to simulate the channel of the shallow sea. The parameters of this simulation are shown in Table 3.

Table 3. The parameters used to establish the model of the shallow sea's channel with Bellhop software.

Sea Depth	Source Depth	Receiving Depth	Sending and Receiving Distance	Speed of Sound	Medium Density	Attenuation Coefficient	Ray Exit Angle
80 m	10 m	14.7 m	129 m	1600 m/s	1500 kg/m^3	0.3 dB/λ	$\pm 30°$

The parameters of the transmitted and received signals are shown in Table 2. The receiver continuously received the signal for a duration of 1 min. When the SNR was -5 dB, the OMP algorithms based on various weighted functions were used to estimate the multipath information of the current channel.

Figure 5 shows the sound-velocity profile used by Bellhop, and Figure 6 exhibits the channel's impulse response at the receiving point. The impulse response indicates that only two sound rays reached the receiving point, with a difference in the delay of 1.4878 ms. Figure 7 presents the estimated results of the different algorithms. In the previous sections, this study showed that the PHAT, SCOT and HB functions exhibited nearly identical performances. Consequently, the PHAT function was chosen as the representative of these three weighted functions.
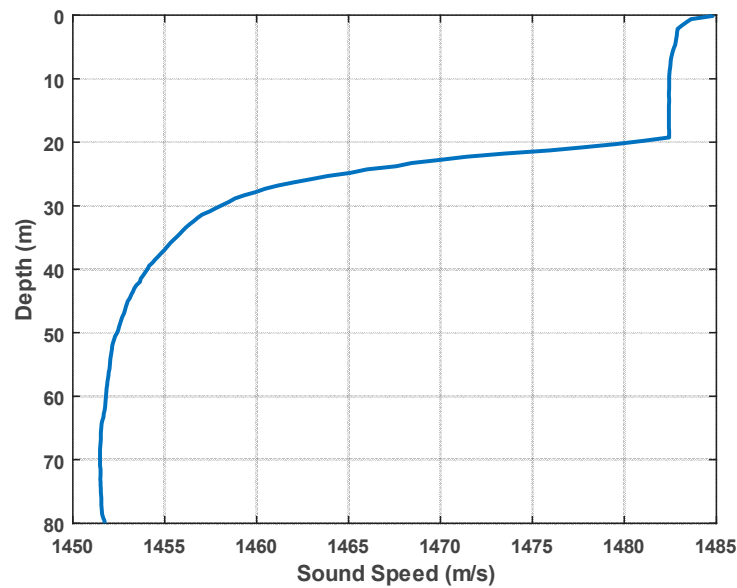
Figure 5. Sound-velocity profile.
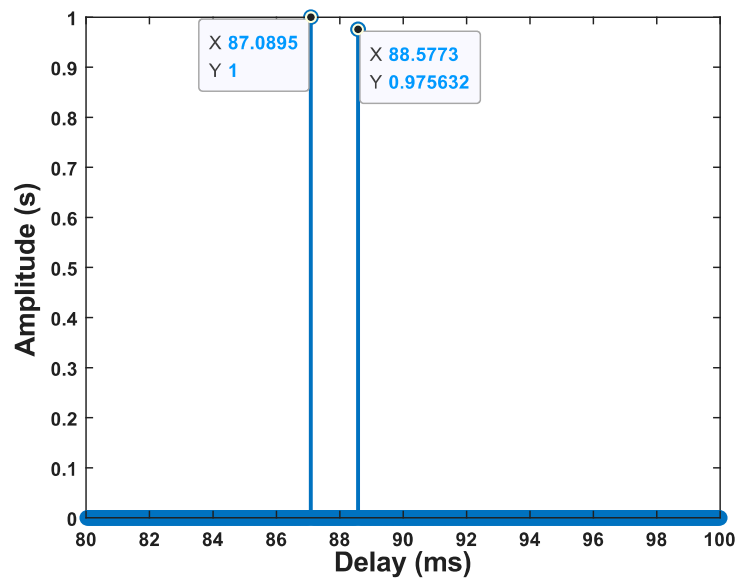
Figure 6. Normalized impulse response of the channel.
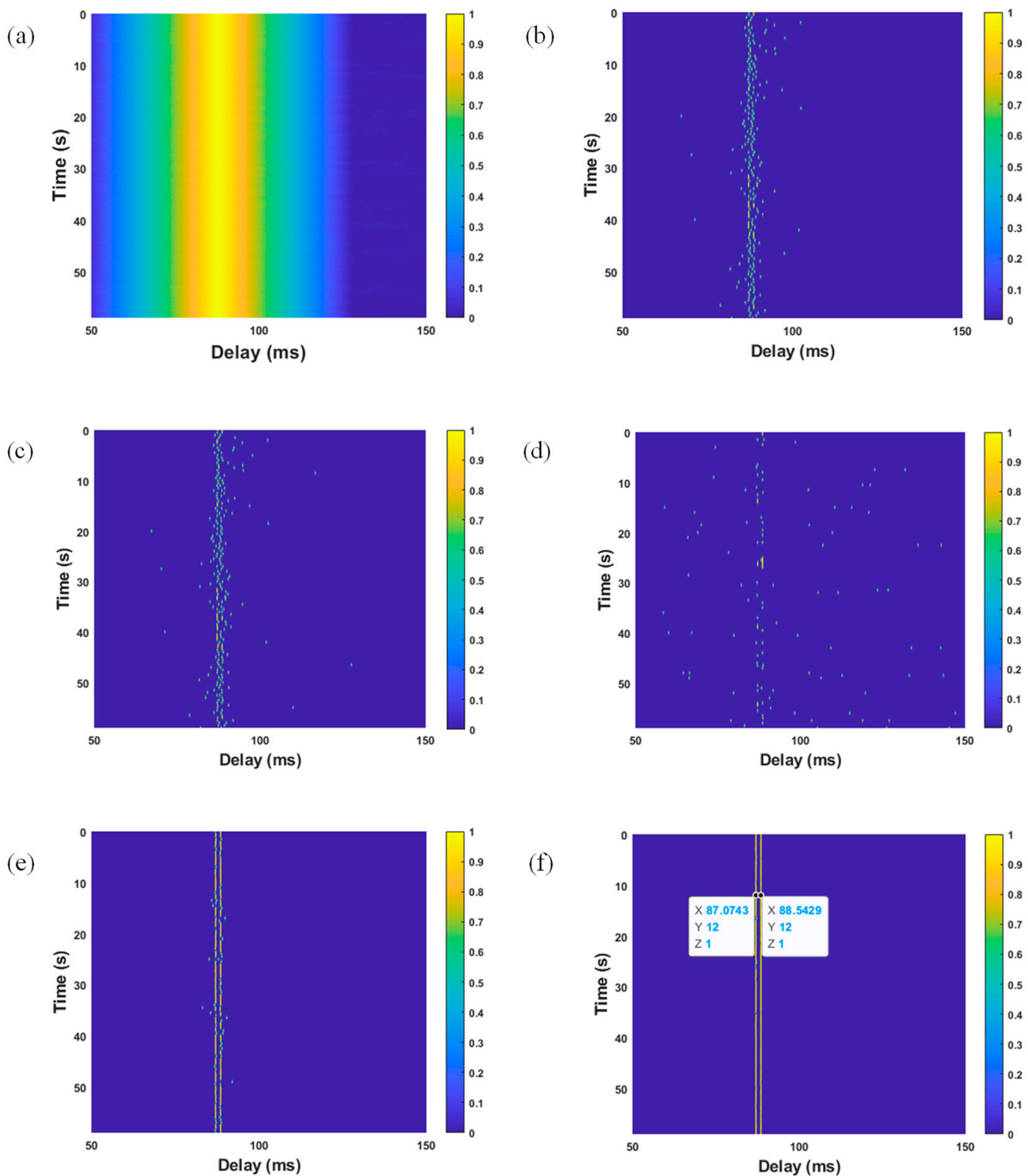
Figure 7. (**a**–**f**) Estimated results of different algorithms: (**a**) matched filtering algorithm; (**b**) classical OMP algorithm; (**c**) GCC-OMP algorithm; (**d**) PHAT-OMP algorithm; (**e**) ROTH OMP algorithm; (**f**) M-PHAT-OMP algorithm.

The results of the simulation indicated that it was challenging to distinguish two multipath delays with a small difference in the delays using the classical OMP algorithm within this simulation environment, and the classical OMP algorithm had the same performance

as the GCC-OMP algorithm. The PHAT-OMP algorithm failed to estimate the delay at this SNR. The ROTH OMP algorithm could estimate two sources of multipath information; however, the estimated results exhibited discontinuities and outliers. The M-PHAT-OMP algorithm proposed in this study estimated two smooth paths with a few outliers, and the estimated delay deviated from the theoretical value by 0.0192 ms, being approximately 1.4915 ms. The results of the simulation confirmed the excellent robustness and resolution of delay of the proposed algorithm.

The relative position of the equipment was changed to further analyze the performance of the proposed algorithm under the condition of more sound lines.

Simulation II: Analyzing the performance of the proposed algorithm with multipath delay

The source depth and receiving depth were both 25 m. The horizontal distance between the sender and receiver was 500 m. All other parameters remained consistent with those in Table 3. Figure 8 shows the channel's impulse response at the receiving point.
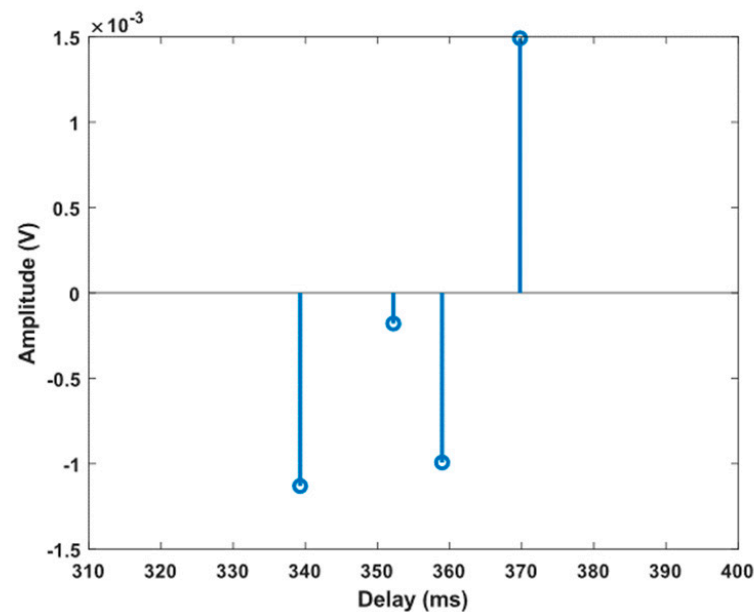

Figure 8. The channel's impulse response.

The parameters of the transmitted and received signals are shown in Table 2. The transmitted signal was propagated through the upper underwater acoustic channel and reached the destination. Gaussian white noise was added to the received signal, and the Monte Carlo simulation method was used to analyze the *RMSE*, NMSE_{PDP} and RFD statistics of the different weighted OMP algorithms.

The curves depicted in Figure 9 indicate that the classical OMP algorithm had the same performance as the GCC-OMP algorithm; however, due to the large amount of computation, the GCC-OMP algorithm was used in the following section to replace the classical OMP algorithm [21]. Under low-SNR conditions, the classical OMP algorithm, which was the same as the GCC-OMP algorithm in this study, exhibited smaller *RMSE* and NMSE_{PDP} values compared with those of the PHAT-OMP and ROTH OMP algorithms. However, its RFD value was higher compared with those of the PHAT-OMP and ROTH OMP algorithms. That is, in low-SNR scenarios, the performances of the commonly weighted OMP algorithms were inferior to that of the classical OMP algorithm. The M-PHAT-OMP algorithm proposed in this study exhibited a superior performance compared with the other algorithms, as evidenced by its lower *RMSE* and NMSE_{PDP} and higher RFD values. The performance of the M-PHAT-OMP algorithm at an SNR of 14 dB surpassed those of the other algorithms at an SNR of 20 dB. In summary, the M-PHAT-OMP algorithm

exhibited a superior performance compared with the classical OMP algorithm and the common weighted OMP algorithms.
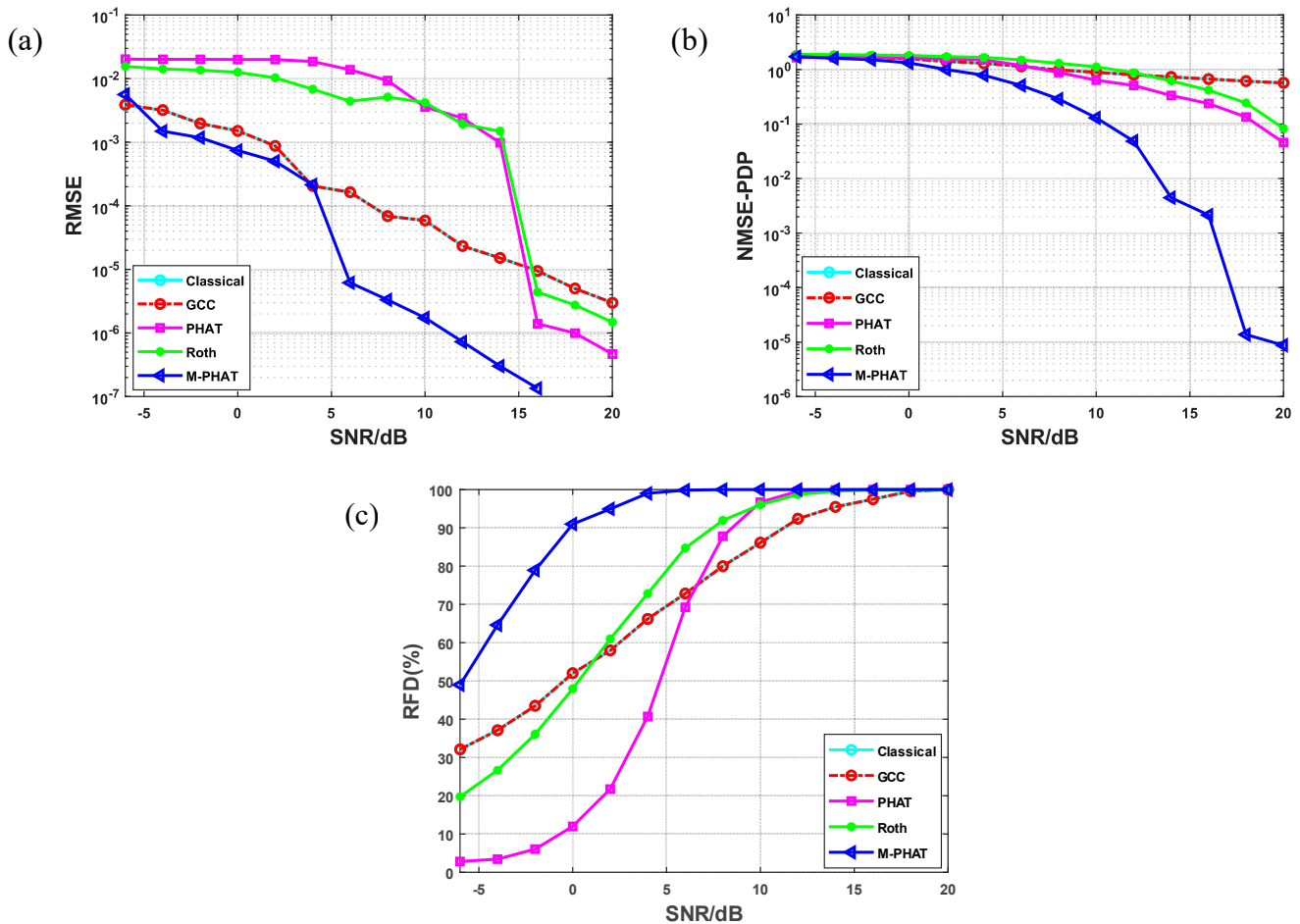

Figure 9. (**a**–**c**) Statistical characteristics of different algorithms: (**a**) *RMSE* with various SNRs; (**b**) NMSE$_{PDP}$ with various SNRs; (**c**) RFD with various SNRs.

3.2.3. Moving Source

The parameters were the same as those in Simulation II, and the source of the signal approached the hydrophone at a velocity of 10 m/s. The performances of the different weighted OMP algorithms were analyzed using the Monte Carlo simulation method when the sound source was moving. The *RMSE*, NMSE$_{PDP}$, NMSE$_{DSSF}$ and RFD statistics under different SNRs are presented in Figure 10.

The curves depicted in Figure 10 demonstrate that when the relative velocity between the transmitter and receiver was 10 m/s, the GCC-OMP algorithm exhibited a convergence in its *RMSE* at 1.4×10^{-4}, indicating that the information on the delay was estimated well. However, the convergence in its RFD was approximately 24.8%, suggesting significant errors in the estimated Doppler factor, and its NMSE$_{PDP}$ and NMSE$_{DSSF}$ converged separately to approximately 1.23 and 1.8, respectively, signifying notable errors in the estimated information on amplitude. The *RMSE* and NMSE$_{PDP}$ of the OMP algorithms based on the PHAT- and ROTH-weighted functions were hardly affected by the SNR, whereas their RFDs increased with a higher SNR. In other words, as the SNR increased, the algorithm's accuracy for estimating the Doppler factor also increased. The *RMSE*, NMSE$_{PDP}$ and NMSE$_{DSSF}$ of the M-PHAT-OMP algorithm's estimations were the smallest when the SNR was greater than 0 dB, and the curve tended to decline with an increase in the SNR. When the SNR was 10 dB, both the *RMSE* and NMSE$_{PDP}$ of the proposed algorithm exhibited superior performances compared with the convergence error of the classical OMP.

The proposed algorithm achieved an RFD of 90% at an SNR of 0 dB, which significantly surpassed the convergence of classical OMP. The results of the simulation demonstrated that the M-PHAT-OMP algorithm maintained a superior performance compared with the other OMP algorithms in the context of a moving sound source.
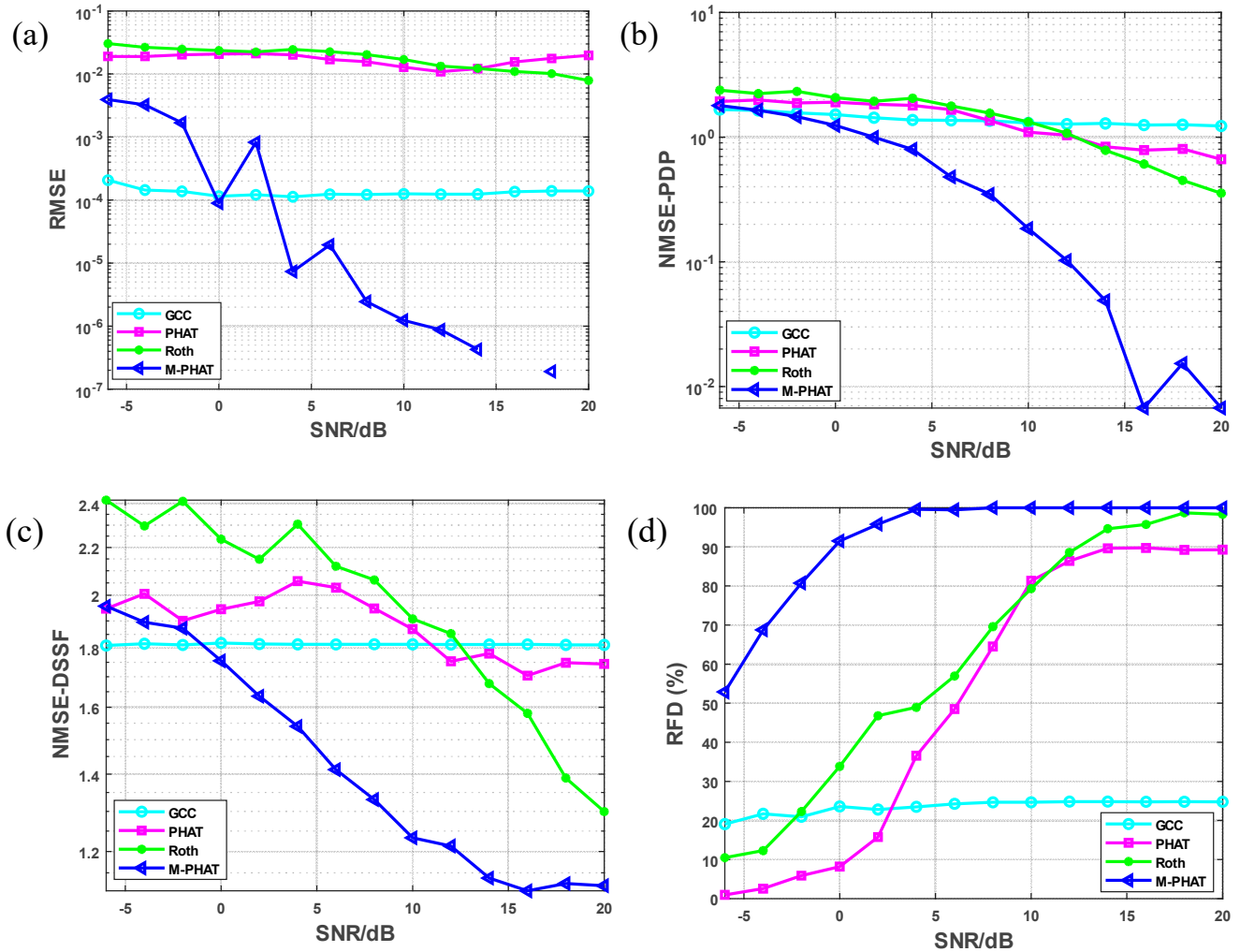

Figure 10. The statistics of different algorithms: (**a**) *RMSE* for various SNRs; (**b**) NMSE$_{PDP}$ for various SNRs; (**c**) NMSE$_{DSSF}$ for various SNRs; (**d**) RFD for various SNRs.

4. Experimental Results

The performance of the M-PHAT-OMP algorithm was analyzed through an experiment under conditions in which the receiver hydrophone remained stationary while the sound source was either fixed or moved.

4.1. Fixed Source

The channel testing experiment was conducted at Lake Qiandao in Hangzhou at the end of November 2022. The experimental setup and the construction of the experimental system are illustrated in Figure 11a,b, and the parameters of the experimental equipment and transmitted signal are shown in Table 4. The gradient of the velocity of the sound measured in the experimental area of the water is depicted in Figure 5.
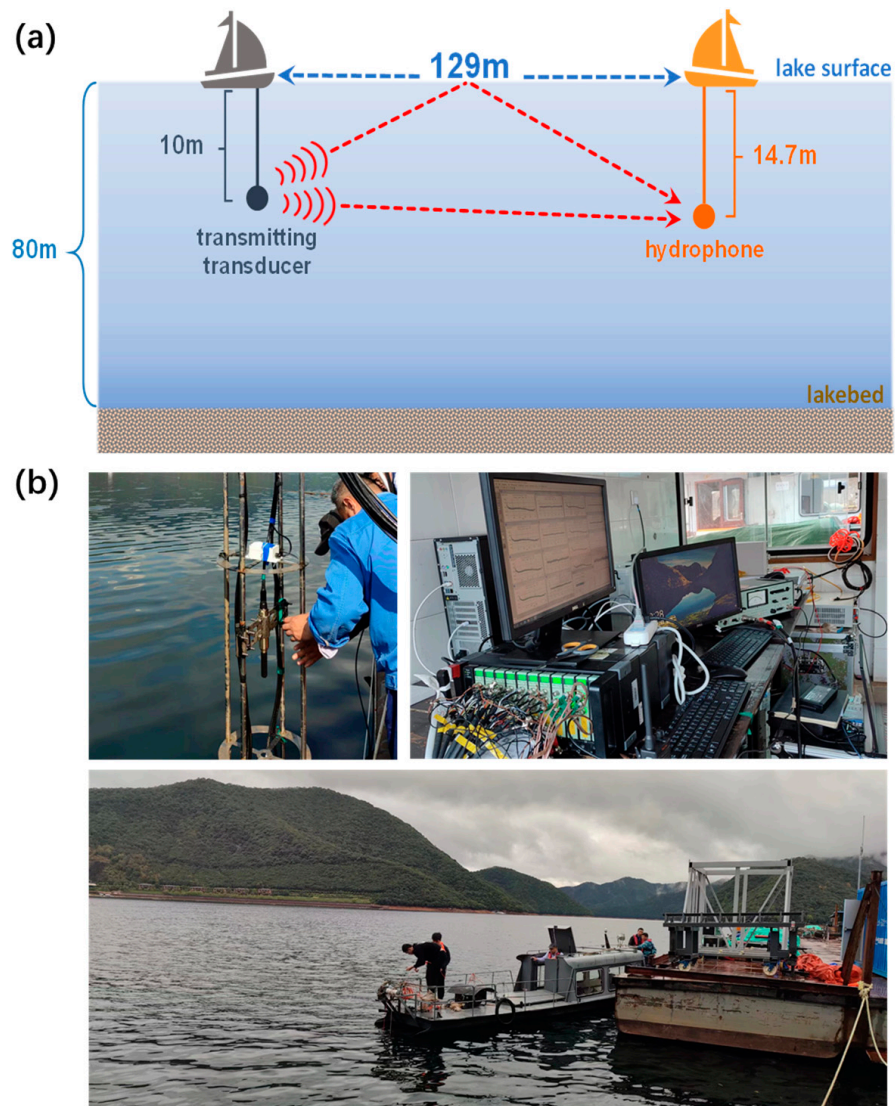
Figure 11. (**a**) Diagram of the experimental setup. (**b**) Construction of the experimental test system used in the lake.

Table 4. The parameters of the experimental equipment and the transmitted signal.

Layout				Transmitted Signal				Received Signal
Lake Depth	Source Depth	Hydrophone Depth	Sending and Receiving Distance	Signal Type	Pulse Width	Frequency	Pulse Period	Sampling Rate
80 m	10 m	14.7 m	129 m	CW pulse	40 ms	25 kHz	500 ms	262.144 kHz

Figure 12 illustrates the results of the simulation and those of processing the experimental data on the time history of the channel's impulse response within 1 min under these particular conditions. According to the analysis of the experimental results shown in Figure 12, the matched filtering algorithm could only estimate one delay path, and its resolution was limited; the estimation results obtained from the GCC-OMP algorithm exhibited oscillations, which hindered its ability to accurately distinguish between the two paths. The PHAT-OMP and ROTH OMP algorithms failed to produce accurate estimations. The M-PHAT-OMP algorithm estimated two smooth multipath paths, and the relative difference in the delay between the two paths was 1.6746 ms, which deviates from the theoretical value by only 0.1873 ms. The experimental results demonstrated that the proposed algorithm exhibited superior robustness and resolution.
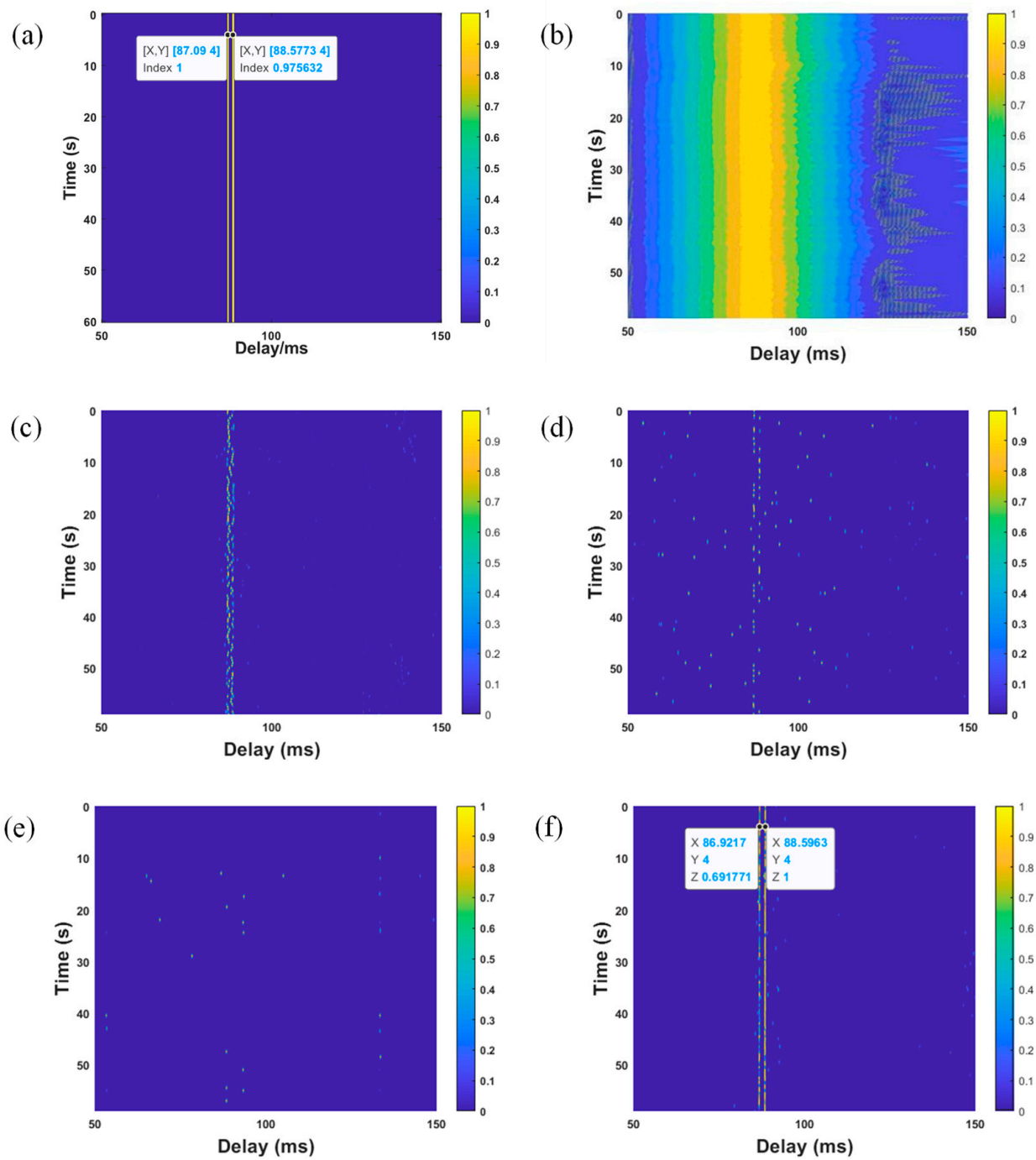
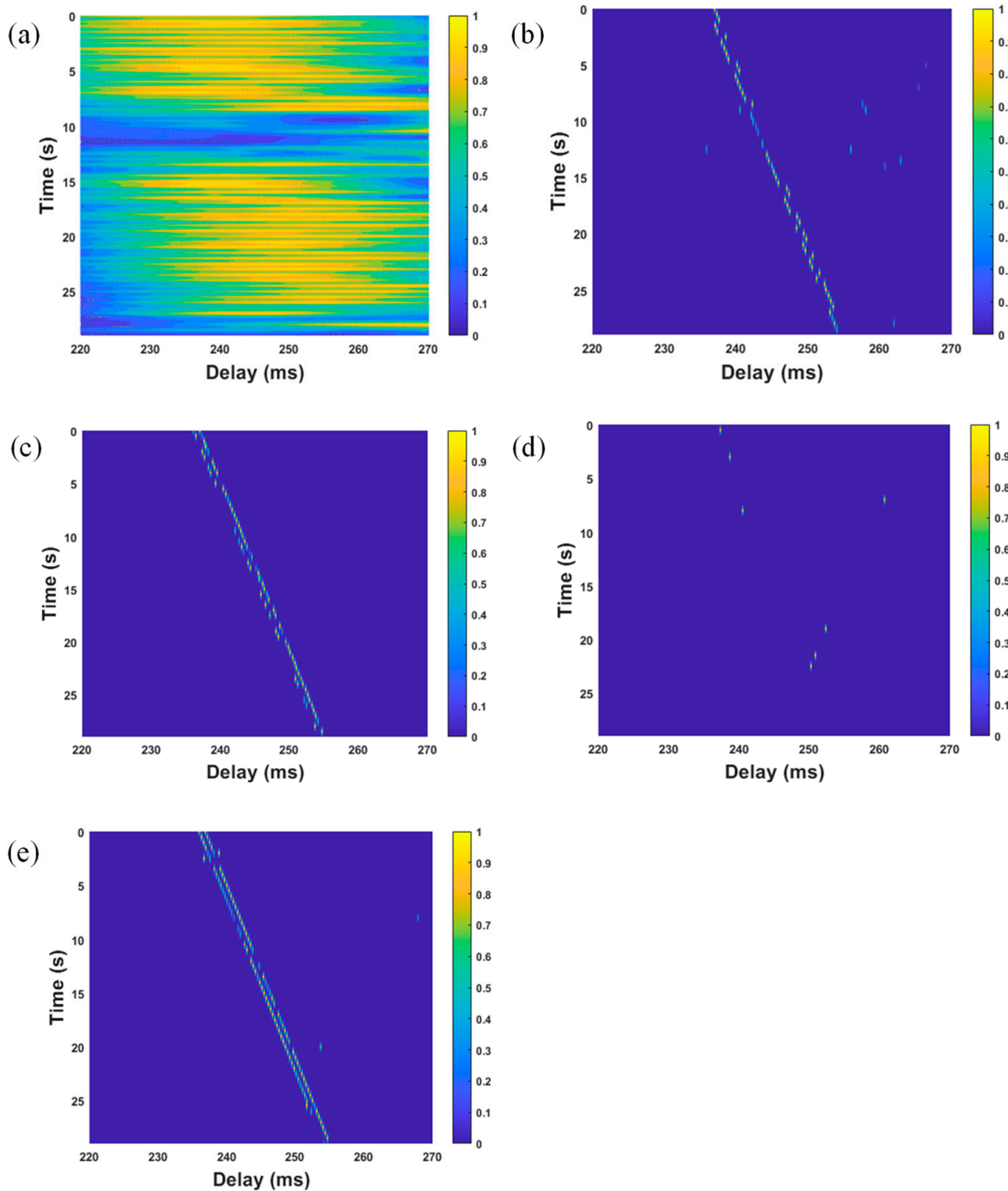**Figure 12.** (**a**) Diagram of the history of the simulated channel's impulse response time. (**b**) Estimation of the channel based on the matched filtering algorithm. (**c**) Estimation of the channel based on the CCC-OMP algorithm. (**d**) Estimation of the channel based on the PHAT-OMP algorithm. (**e**) Estimation of the channel based on the ROTH OMP algorithm. (**f**) Estimation of the channel based on the M-PHAT-OMP algorithm.

4.2. Moving Sound Source

The ship carried the transmitting transducer away from the receiving hydrophone at a speed of 1 m/s. The parameters of the experimental setup and the transmitted signal are shown in Table 5. The experimental results are presented in Figure 13:

Table 5. The parameters of the experimental layout and the transmitted signal.

Layout				Transmitted Signal				Received Signal
Lake Depth	Source Depth	Hydrophone Depth	Sending and Receiving Distance	Signal Type	Pulse Width	Frequency	Pulse Period	Sampling Rate
80 m	20 m	14.7 m	350 m	CW pulse	40 ms	20 kHz	500 ms	262.144 kHz

Figure 13. (**a**) Estimation of the channel based on the matched filtering algorithm. (**b**) Estimation of the channel based on the GCC-OMP algorithm. (**c**) Estimation of the channel based on the PHAT-OMP algorithm. (**d**) Estimation of the channel based on the ROTH OMP algorithm. (**e**) Estimation of the channel based on the M-PHAT-OMP algorithm.

The analysis of the experimental results indicated that neither the matched filtering algorithm nor the GCC-OMP algorithm could distinguish between the two paths, and the estimated paths were discontinuous. The ROTH OMP algorithm failed to estimate the paths. The PHAT-OMP algorithm could estimate two paths; however, it was unstable and failed to estimate the corresponding delay at most time points. The M-PHAT-OMP algorithm clearly distinguished the two paths, and the relative difference in the delay was about 0.8 ms. The estimated speed of this algorithm was approximately 1 m/s, which was in close agreement with the predetermined speed. The estimated results of the M-PHAT-OMP algorithm exhibited greater resolution and superior robustness compared with the aforementioned algorithms.

5. Conclusions

According to the situation of using narrowband signals to estimate the channel information in active sonar, this study proposed a modified PHAT-weighted OMP algorithm (M-PHAT-OMP). This algorithm is essentially a combination of the fundamental frequency-domain OMP algorithms and the modified PHAT-weighted GCC algorithm. In this study, a model of a channel in a shallow sea was established to investigate the performance of the algorithm under scenarios with stationary and moving sound sources. In each iteration, the M-PHAT-OMP algorithm updated the index set with the index corresponding to the peak value of the improved PHAT-weighted GCC algorithm, which not only reduced the computational burden, but also reduced the $RMSE$, $NMSE_{PDP}$ and $NMSE_{DSSF}$ and improved the RFD estimated by the algorithm. The simulation results and the analysis of the test data of Lake Qiandao demonstrated that the proposed algorithm exhibited superior robustness and better resolution of the time delay and environmental adaptability than the classical algorithm under the scenarios of static and dynamic sound sources.

In our upcoming research, we aim to apply the algorithm in more intricate deep-water channels and challenging sea conditions, and to explore its robustness in the presence of significant Doppler shifts in the received signal on a large scale.

References

1. Stojanovic, M.; Preisig, J. Underwater acoustic communication channels: Propagation models and statistical characterization. *IEEE Commun. Mag.* **2009**, *47*, 84–89. [CrossRef]
2. Zhou, Y.; Song, A.; Tong, F. Underwater acoustic channel characteristics and communication performance at 85 kHz. *J. Acoust. Soc. Am.* **2017**, *142*, EL350. [CrossRef] [PubMed]
3. Yang, T.C. Properties of underwater acoustic communication channels in shallow water. *J. Acoust. Soc. Am.* **2012**, *131*, 129–145. [CrossRef] [PubMed]
4. Murad, M.; Sheikh, A.A.; Manzoor, M.A.; Felemban, E.; Qaisar, S. A Survey on Current Underwater Acoustic Sensor Network Applications. *Int. J. Comput. Theory Eng.* **2014**, *7*, 51–56. [CrossRef]
5. Li, W.; Preisig, J.C. Estimation of Rapidly Time-Varying Sparse Channels. *IEEE J. Ocean. Eng.* **2007**, *32*, 927–939. [CrossRef]
6. Van De Beek, J.-J.; Edfors, O.; Sandell, M.; Wilson, S.K.; Borjesson, P.O. On channel estimation in OFDM systems. In Proceedings of the 1995 IEEE 45th Vehicular Technology Conference. Countdown to the Wireless Twenty-First Century, Chicago, IL, USA, 25–28 July 1995; pp. 815–819.

7. Seung Joon, L. On the training of MIMO-OFDM channels with least square channel estimation and linear interpolation. *IEEE Commun. Lett.* **2008**, *12*, 100–102. [CrossRef]
8. Jones, V.; Raleigh, G.C. Channel estimation for wireless OFDM systems. In Proceedings of the IEEE GLOBECOM 1998 (Cat. NO. 98CH36250), Sydney, NSW, Australia, 8 December 1998; pp. 980–985.
9. Edfors, O.; Sandell, M.; Van de Beek, J.-J.; Wilson, S.K.; Borjesson, P.O. OFDM channel estimation by singular value decomposition. *IEEE Trans. Commun.* **1998**, *46*, 931–939. [CrossRef]
10. Berger, C.R.; Shengli, Z.; Preisig, J.C.; Willett, P. Sparse Channel Estimation for Multicarrier Underwater Acoustic Communication: From Subspace Methods to Compressed Sensing. *IEEE Trans. Signal Process.* **2010**, *58*, 1708–1721. [CrossRef]
11. Donoho, D.L. Compressed sensing. *IEEE Trans. Inf. Theory* **2006**, *52*, 1289–1306. [CrossRef]
12. Lu, S.; Hemadeh, I.A.; El-Hajjar, M.; Hanzo, L. Compressed-Sensing-Aided Space-Time Frequency Index Modulation. *IEEE Trans. Veh. Technol.* **2018**, *67*, 6259–6271. [CrossRef]
13. Knill, C.; Schweizer, B.; Sparrer, S.; Roos, F.; Fischer, R.F.H.; Waldschmidt, C. High Range and Doppler Resolution by Application of Compressed Sensing Using Low Baseband Bandwidth OFDM Radar. *IEEE Trans. Microw. Theory Tech.* **2018**, *66*, 3535–3546. [CrossRef]
14. Zhou, Y.-h.; Tong, F.; Zhang, G.-Q. Distributed compressed sensing estimation of underwater acoustic OFDM channel. *Appl. Acoust.* **2017**, *117*, 160–166. [CrossRef]
15. Yang, L.; Song, K.; Siu, Y.M. Iterative Clipping Noise Recovery of OFDM Signals Based on Compressed Sensing. *IEEE Trans. Broadcast.* **2017**, *63*, 706–713. [CrossRef]
16. Karabulut, G.Z.; Yongacoglu, A. Sparse channel estimation using orthogonal matching pursuit algorithm. In Proceedings of the IEEE 60th Vehicular Technology Conference, Los Angeles, CA, USA, 26–29 September 2004; VTC2004-Fall; pp. 3880–3884.
17. Qiao, G.; Qiang, X.; Wan, L. Double Interpolation-Based Linear Fitting for OMP Channel Estimation in OFDM Systems. *IEEE Commun. Lett.* **2021**, *25*, 2908–2912. [CrossRef]
18. Tao, J.; Qi, C.; Huang, Y. Regularized Multipath Matching Pursuit for Sparse Channel Estimation in Millimeter Wave Massive MIMO System. *IEEE Wirel. Commun. Lett.* **2019**, *8*, 169–172. [CrossRef]
19. Lei, Z.; Chunting, Q. Newton pursuit algorithm for sparse signal reconstruction in compressed sensing. In Proceedings of the 2010 3rd International Conference on Computer Science and Information Technology, Chengdu, China, 9–11 July 2010; pp. 463–466.
20. Die, H.; Xiaodong, W.; Lianghua, H. A New Sparse Channel Estimation and Tracking Method for Time-Varying OFDM Systems. *IEEE Trans. Veh. Technol.* **2013**, *62*, 4648–4653. [CrossRef]
21. Yu, F.; Li, D.; Guo, Q.; Wang, Z.; Xiang, W.J.I.C.L. Block-FFT based OMP for compressed channel estimation in underwater acoustic communications. *IEEE Commun. Lett.* **2015**, *19*, 1937–1940. [CrossRef]
22. Wan, L.; Qiang, X.; Ma, L.; Song, Q.; Qiao, G. Accurate and Efficient Path Delay Estimation in OMP Based Sparse Channel Estimation for OFDM With Equispaced Pilots. *IEEE Wirel. Commun. Lett.* **2019**, *8*, 117–120. [CrossRef]
23. Ma, L.; Li, T.; Liu, S.; Qiao, G.; Jia, H. Efficient interpolation based OMP for sparse channel estimation in underwater acoustic OFDM. *Appl. Acoust.* **2021**, *172*, 107606. [CrossRef]
24. Qiao, G.; Song, Q.; Ma, L.; Wan, L. A low-complexity orthogonal matching pursuit based channel estimation method for time-varying underwater acoustic OFDM systems. *Appl. Acoust.* **2019**, *148*, 246–250. [CrossRef]
25. Li, C.; Song, K.; Yang, L. Low computational complexity design over sparse channel estimator in underwater acoustic OFDM communication system. *IET Commun.* **2017**, *11*, 1143–1151. [CrossRef]
26. Zhou, Y.; Zeng, F.-Z.; Gu, Y.-C. A gradient descent sparse adaptive matching pursuit algorithm based on compressive sensing. In Proceedings of the 2016 International Conference on Machine Learning and Cybernetics (ICMLC), Jeju, Republic of Korea, 10–13 July 2016; pp. 464–469.
27. Wang, Z.; Li, Y.; Wang, C.; Ouyang, D.; Huang, Y. A-OMP: An Adaptive OMP Algorithm for Underwater Acoustic OFDM Channel Estimation. *IEEE Wirel. Commun. Lett.* **2021**, *10*, 1761–1765. [CrossRef]
28. Zhang, Y.; Venkatesan, R.; Dobre, O.A.; Li, C. An adaptive matching pursuit algorithm for sparse channel estimation. In Proceedings of the 2015 IEEE Wireless Communications and Networking Conference (WCNC), New Orleans, LA, USA, 9–12 March 2015; pp. 626–630.
29. Sun, Q.; Wu, F.-Y.; Yang, K.; Ma, Y. Estimation of multipath delay-Doppler parameters from moving LFM signals in shallow water. *Ocean Eng.* **2021**, *232*, 109125. [CrossRef]
30. Wang, Z.; Wu, H.; Liu, S. An improved sparse underwater acoustic OFDM channel estimation method based on joint sparse model and exponential smoothing. In Proceedings of the 2017 IEEE International Conference on Signal Processing, Communications and Computing (ICSPCC), Xiamen, China, 22–25 October 2017; pp. 1–6.
31. Padois, T.; Doutres, O.; Sgard, F. On the use of modified phase transform weighting functions for acoustic imaging with the generalized cross correlation. *J. Acoust. Soc. Am.* **2019**, *145*, 1546. [CrossRef] [PubMed]
32. Xu, L.; Chen, L.; Li, Y.; Jiang, W. A Block Sparse-Based Dynamic Compressed Sensing Channel Estimator for Underwater Acoustic Communication. *J. Mar. Sci. Eng.* **2022**, *10*, 536. [CrossRef]
33. Knapp, C.; Carter, G. The generalized correlation method for estimation of time delay. *IEEE Trans. Acoust. Speech Signal Process.* **1976**, *24*, 320–327. [CrossRef]

34. Li, C.Z.; Shao, F.Q.; Kan, Z.; Fan, H.X. The Generalized Cross-Power Spectrum Method for Estimation of Time Delay in Acoustic Pyrometer. *Appl. Mech. Mater.* **2011**, *88–89*, 615–620. [CrossRef]
35. Zhao, Y.; Yu, H.; Wei, G.; Ji, F.; Chen, F.; Zhang, J. FRFT-based parameter estimation of time-varying wideband underwater acoustic multipath channels. In Proceedings of the 10th International Conference on Underwater Networks & Systems, Arlington, VA, USA, 22–24 October 2015; pp. 1–8.
36. Ye, J.; Papandreou-Suppappola, A. Discrete time-scale characterization of wideband time-varying systems. *IEEE Trans. Signal Process.* **2006**, *54*, 1364–1375. [CrossRef]
37. Zhao, Y.; Yu, H.; Wei, G.; Ji, F.; Chen, F. Parameter Estimation of Wideband Underwater Acoustic Multipath Channels based on Fractional Fourier Transform. *IEEE Trans. Signal Process.* **2016**, *64*, 5396–5408. [CrossRef]